



Curved Polymeric Sandwich Composites Subjected to Air Shock: An Experimental Investigation

A. Pandey¹ · P. Wanchoo¹ · H. Matos¹ · A. Shukla¹

Received: 30 January 2024 / Accepted: 8 April 2024
© The Author(s) 2024

Abstract

Background The vulnerability of polymeric composite sandwich structures in marine applications to air explosions highlights a significant gap in our understanding of the dynamic behavior of the curved sandwich structures, which is essential for design improvements.

Objective This study aims to explore the dynamic response and failure mechanisms of curved sandwich composite panels subjected to air-blast loading, providing insights into their structural integrity under such conditions.

Methods Experiments were performed using laboratory-simulated air shocks generated by a shock tube, employing high-speed photography and digital image correlation to measure deflections on the back surface of the panels. The panels, made with PVC closed-cell foam cores of two densities (H45 and H130), were tested across three curved geometries (radii of 112 mm, 305 mm, and infinity) under various boundary conditions.

Results Findings indicate an increase in deformation with a decreased radius of curvature under simple support conditions, a trend that reverses under arrested displacement conditions. Moreover, a reduced radius significantly enhances panel strength and resistance to interfacial damage, with the primary failure mode transitioning from core shear cracking to interfacial debonding as core density increases.

Conclusions The study reveals that the radius of curvature, boundary conditions, and core density significantly affect curved sandwich panels' dynamic response and performance. Panels with smaller radii and higher core densities exhibit increased strength, though boundary conditions introduce variable effects on deformation behavior.

Keywords Sandwich composites · Curved structures · Blast loading · Shock loading · Progressive damage

Introduction

Polymeric sandwich composites are prominent solutions for building marine structures. These structural systems are also comprised of curved sections, such as the bow of a ship, that are typically the first to be exposed to external loadings [1]. Utilizing a sandwich composite design allows these ships to achieve strength comparable to their metal counterparts while significantly reducing weight and enhancing

stealth properties. As a result, contemporary naval ships are increasingly adopting these materials for constructing light-weight ship hulls and superstructures. Due to the potential vulnerability of these structures to blast-induced loads from explosions or other high-energy sources, it's imperative to engineer them to withstand these extreme forces without catastrophic failure. The sandwich composite structure, consisting of two thin and stiff facesheets with a softer core material in between, serves this purpose. In blast mitigation, the loss of structural integrity is not a desirable outcome. The catastrophic damage in the context of these sandwich structures is the facesheet failure, causing the disintegration of the structure. The design of a sandwich composite structure is analogous to the cross-section of an I-beam wherein the facesheet bears flexural loads while the core manages transverse shear loads.

Various experimental studies have deepened our understanding of the response of composite structures under blast

A. Shukla, A. Pandey, P. Wanchoo and H. Matos are members of SEM.

✉ A. Shukla
shuklaa@uri.edu

¹ Dynamic Photo-Mechanics Laboratory, Department of Mechanical, Industrial and Systems Engineering, University of Rhode Island, Kingston, RI, USA

loading conditions. Researchers have proposed passive techniques to improve blast performance, such as higher impedance mismatch at interfaces, graded core sandwiches, protective sacrificial cladding, laminate stacking with hybrid interlaminar material configurations, and techniques for redirecting or disrupting the blast wave [2–6]. Significant contributions have also been made to characterize the dynamic response of polymeric sandwich composite structures to in-air blast loading through experiments. For instance, Wang et al. [7, 8] performed laboratory-scale air shock loading experiments on sandwich beam specimens, revealing that specific configurations of better-dissipated energy and in-plane compressive loads increase the damage to the face sheet exposed to blast. Gardner et al. [9, 10] and Tekalur et al. [11] experimented with various sandwich panel configurations to improve blast performance. Alanbay et al. [12] analyzed multilayered sandwich composite structures using a surrogate modeling-based optimization algorithm and developed optimal core layout configurations for minimum deflections and transmitted force.

Curved geometries are essential in naval structures due to design and manufacturing requirements, necessitating understanding the geometric effects of curved sandwich composite structures under shock loading. Previous studies, such as those by Kardomateas et al. [13], Rodcheuy et al. [14], Pradyumna et al. [15], and Hoo Fatt et al. [16], have developed various theories and models to predict the dynamic behavior of curved sandwich structures. However, limited experimental investigations exist on curved composite panels exposed to blast loading. When loaded with a shock tube, Kumar et al. [17] found that curved carbon fiber-reinforced plastic laminates increased energy dissipation. Other researchers, like Langdon et al., Jing et al., and Shen et al. [18–20], reported similar findings on the dynamic behavior of curved sandwich panels under blast loading. Yet, most of the literature on curved sandwich panels has focused on postmortem observations.

This investigation captured the real-time blast response of curved sandwich composite panels with different curvatures under blast-induced impulsive loading. The panels, consisting of a carbon fiber facesheet and a closed-cell PVC foam core, were tested using a shock tube apparatus. The study focuses on the following aspects –

1. Quantification of impulse transferred due to planar shock loading on single curve panels.
2. Influence of curvature and boundary conditions together on the dynamic response.
3. Role of core density on the failure of curved sandwich panels.
4. Damage progression and postmortem observations in sandwich panels.

The results reveal that for a given impulsive loading on the curved sandwich panels with simple edge support at boundary, deformation increases with the decrease in radius of curvature. However, with arrested displacement at boundary, there is reversal in the deformation trend. The sandwich panel with the least radius of curvature showed increase in the failure threshold and capability to resist interfacial damage. The increase in the density of core material resulted in transition of primary failure mode from shear cracking in the core to interfacial debond.

Materials and Experimental Methods

Specimen Design and Manufacturing

Specimen geometry selection

The sandwich composite panels chosen for this study measured 200 mm wide, with a 2 mm thick facesheet and a 9.5 mm thick core. The curvature radius of these panels was selected based on the principal area moment of inertia for a curved cross-sectional sandwich. Equations (1) and (2) were employed to evaluate this curved cross-section's area moment of inertia. Notably, the core's contribution to the area moment of inertia was disregarded since its modulus was considerably smaller than that of the facesheet material.

$$I_{yy} = \frac{R_4^4 - R_3^4 + R_2^4 - R_1^4}{8} (2\theta - \sin 2\theta) \quad (1)$$

$$I_{zz} = \frac{R_4^4 - R_3^4 + R_2^4 - R_1^4}{8} (2\theta + \sin 2\theta) - \frac{4}{3} (R_4^3 - R_3^3 + R_2^3 - R_1^3) (\bar{y} \sin \theta) + (R_4^2 - R_3^2 + R_2^2 - R_1^2) (\bar{y}^2 \theta) \quad (2)$$

where R_1 , R_2 , R_3 , and R_4 are the inner and outer radius of the bottom and top facesheet ($R_1 < R_2 < R_3 < R_4$), \bar{y} is the centroid distance of the curved cross-section sandwich composite from the center of curvature, and 2θ is the angle subtended by the extreme edges at the center of the curved section. Figure 1(a) shows a schematic with the geometric details of a curved section.

The area moment of inertia (I_{yy} and I_{zz}) was evaluated for the 178 mm wide curved cross-section sandwich with a 2 mm thick facesheet and 9.5 mm thick core. The variation of the area moment of inertia with the inner radius of the curved section is shown in Fig. 1(b).

It was observed that when the inner radius is 600 mm or greater, the area moment of inertia closely resembles that of

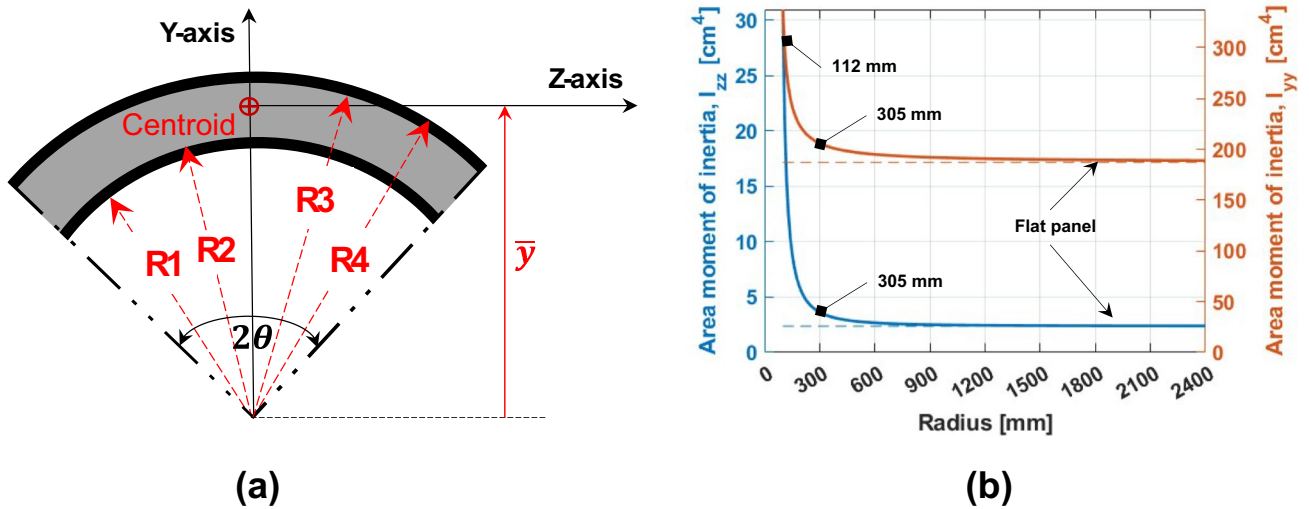


Fig. 1 (a) Sketch of curved cross-section (b) Area moment of inertia variation with inner radius for curved cross-section

a rectangular cross-section, which is indicated by a dashed line in Fig. 1(b). However, the area moment of inertia exhibits an exponential increase when the curved cross-section has an inner radius of less than 300 mm. For the scope of this study, we chose two curved sandwich panels with inner radii of 112 mm and 305 mm, in addition to a flat sandwich panel. This selection encompasses a wide range of area moment of inertia values, as depicted in Fig. 1(b).

In subsequent sections, the sandwich panels with inner radii of 112 mm, 305 mm, and infinity (representing the flat panel) are denoted as Panel A, Panel B, and Panel C, respectively. Figure 2 provides a schematic representation of the three chosen curved sandwich specimens, showcasing their specific dimensions. This figure also illustrates the distances (L) between the straight edges for the two boundary conditions (BC1 and BC2) used in

this research, labeled as ‘L1’ and ‘L2’, respectively. An in-depth explanation of these boundary conditions can be found in "Experimental Setup" section.

Specimen manufacturing

The sandwich specimens were manufactured in-house using the closed-cell PVC (Divinycell® vinyl) foam provided by DIAB International (Laholm, Sweden) as the core. Woven carbon fiber (balanced, twill) prepreps produced by GURIT (Albacete, Spain) were utilized to fabricate the face sheets. The study used foam sheets with a thickness of 9.5 mm and two distinct density grades: H45 and H130. An epoxy-based resin film adhesive from GURIT was chosen to bond the face-sheet to the core. These material details can be found in Table 1. The PVC foam core was thermoformed to achieve

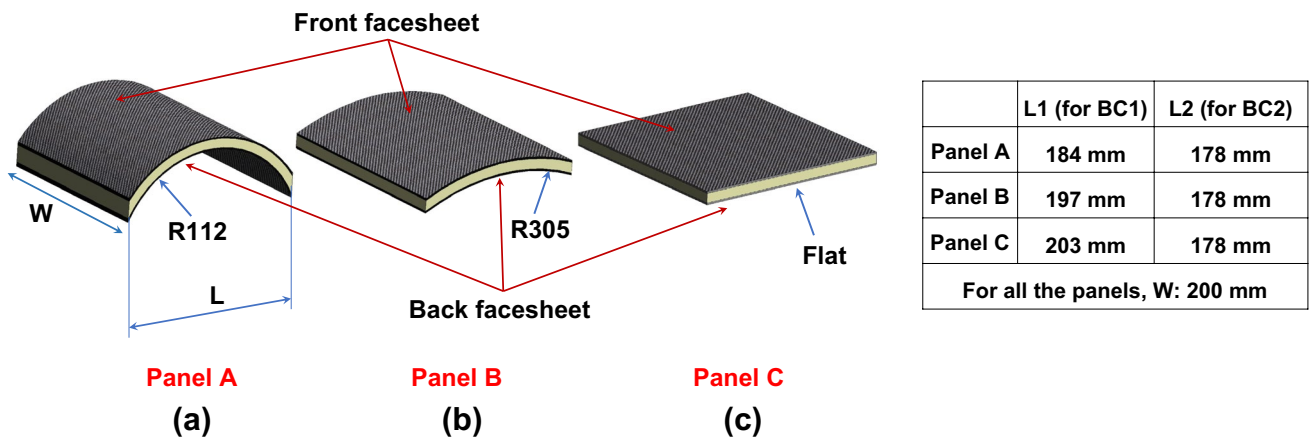


Fig. 2 (a) R112- Panel A (b) R305- Panel B (c) Flat- Panel C

Table 1 Raw material specification and properties

	Specification	Density
Facesheet	Twill woven prepreg (balanced)	416 gsm [22]
Core	H45	$52.1 \pm 0.3 \text{ kg/m}^3$
	H130	$143.9 \pm 0.5 \text{ kg/m}^3$
Film adhesive	ST94	130 gsm

the desired curves. This process involved heating the foam sheets to a temperature of 5 °C below their maximum permissible processing temperatures [21] and pressing them into a thermoforming mold for 30 min.

The sandwich specimens were fabricated through the vacuum bag molding process. This entailed co-curing the woven prepreg with the thermoformed core, incorporating adhesive film at the interfaces. The curing was performed at 85 °C for 9 hours, with a sustained vacuum pressure of 1 bar. Details of the manufacturing method, accompanied by process parameters and images of representative sandwich specimens, are presented in Fig. 3.

Experimental Setup

The sandwich panels were subjected to air shock loading, and their dynamic response was captured on the back face

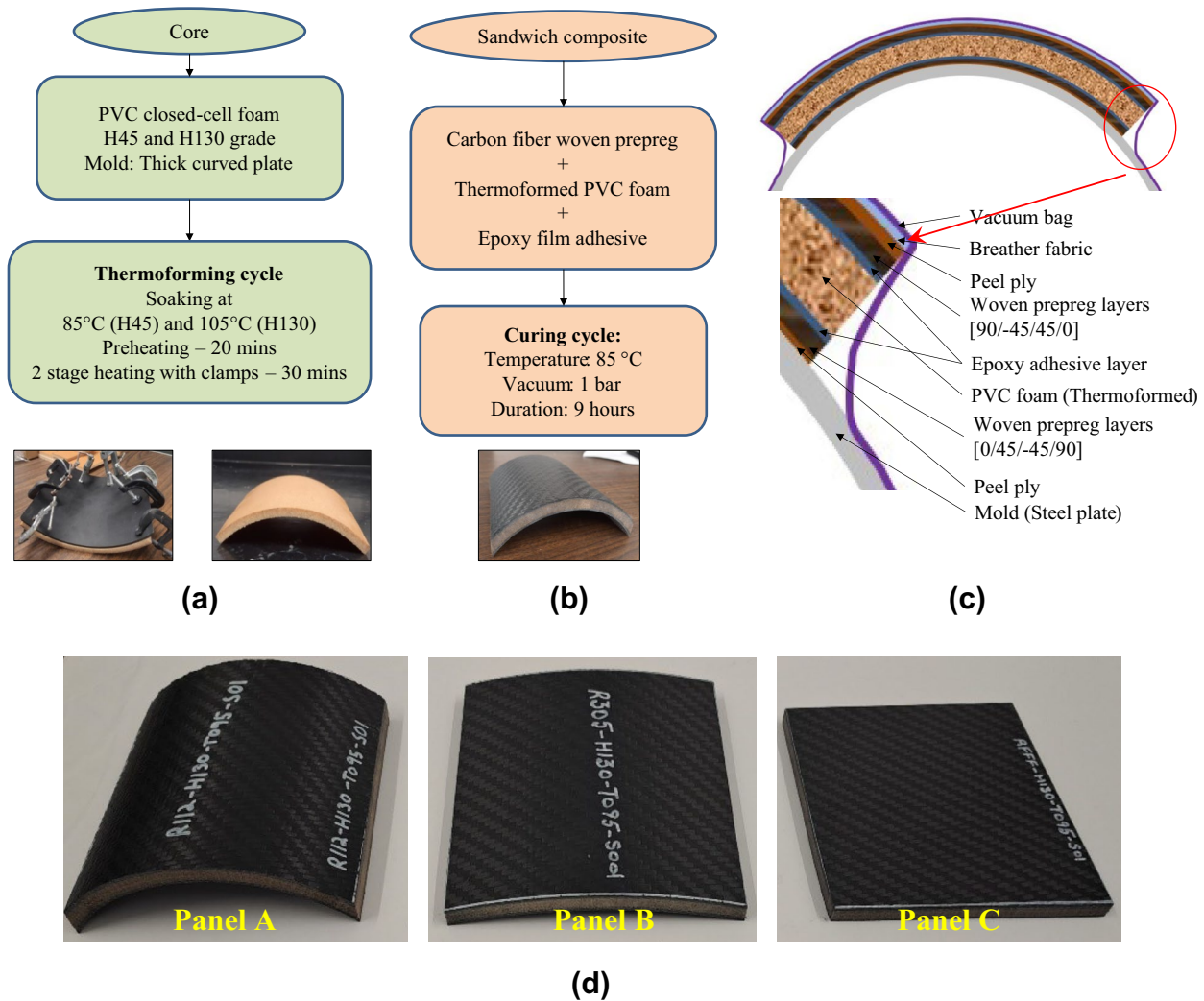
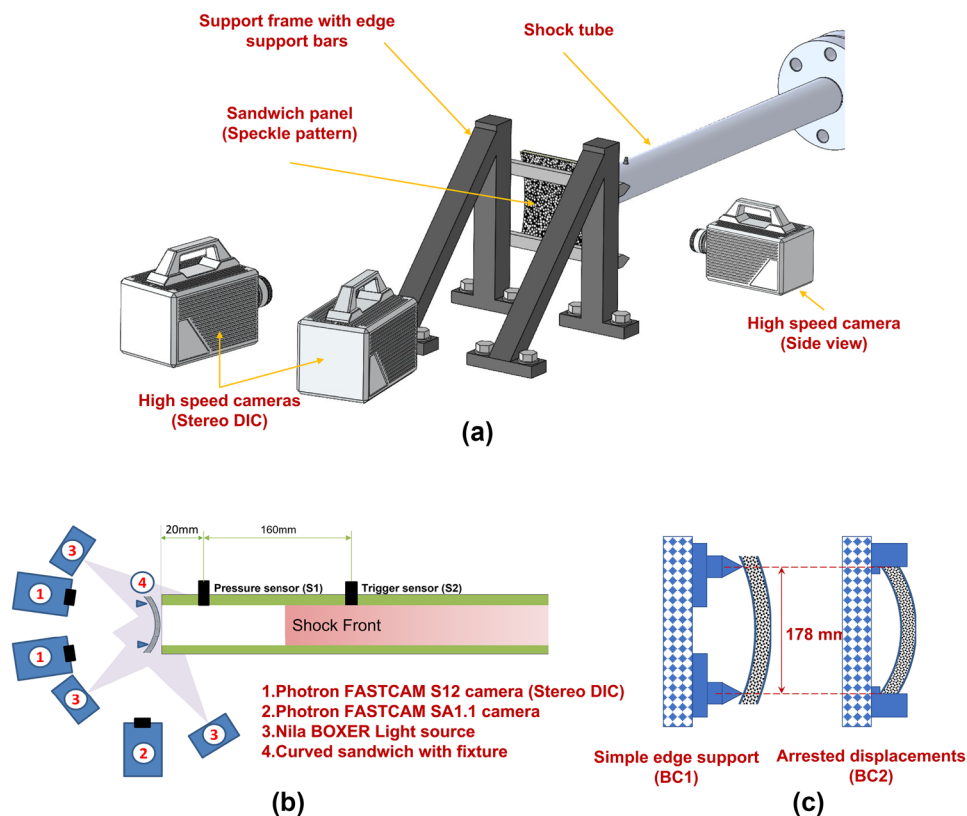


Fig. 3 Manufacturing process for sandwich composite panels (a) Thermoforming process (b) Curing cycle for sandwich panel (c) Schematic of vacuum bag molding process (d) Manufactured specimens (typical)

Fig. 4 (a) Experiment setup— shock tube, the specimen with fixture assembly and high-speed cameras, (b) 2D schematic of experiment setup, and (c) Boundary conditions (BC1 & BC2)



sheet (opposite the loading face) using a high-speed stereo DIC (Digital Image Correlation) method. Figure 4 illustrates a schematic of the experimental setup, highlighting its essential components, such as the shock loading apparatus, specimen boundary conditions, high-speed imaging mechanisms, and the application of DIC.

Shock loading apparatus

The study used a shock tube apparatus to produce controlled planar shock waves for loading the specimens. This shock tube is primarily divided into a brief driver section and an extended driven section, possessing a circular cross-section. The tube stretches over a length of 7 m. The inner diameters of the driver and driven sections measure 0.15 m, while the muzzle section near the loading end has a diameter of 0.076 m. A stiff diaphragm membrane of mylar sheets separates the driver and driven sections. Pressuring the driver section until the membrane ruptures, the gas within quickly surges into the driven section. This abrupt motion generates a pressure pulse, culminating in a planar shock wave front. This shock wave then travels through the shock tube’s muzzle, making contact and applying pressure to the specimen. A more detailed explanation of the operations of this apparatus can be found in previous work [23].

Boundary conditions and loading

The sandwich specimens, with their convex surfaces facing the shock tube muzzle, were held in place using a fixture, as illustrated in Fig. 4. This study employed two distinct fixtures to assess the impact of boundary conditions. Figure 4(c) provides schematics of both fixtures, simulating two different boundary conditions: “Simple edge support” and “Arrested displacements” at the straight edges. For the simple edge support boundary condition, only the horizontal movement of the sandwich specimens was restrained. However, in the arrested displacements boundary condition, horizontal and vertical movements at the straight edges of the plates were inhibited, effectively eliminating any motion in these directions. In the subsequent sections, the boundary conditions of simple edge support and arrested displacements are referred to as ‘BC1’ and ‘BC2’, respectively.

To assess the effect of boundary conditions on the panel’s response without causing damage under air shock loading, specimens with the ‘BC1’ as well as ‘BC2’ boundary conditions underwent a low-intensity shock named ‘LS’, which had an approximate incident shock peak pressure magnitude of 0.5 MPa. Further, only the ‘BC1’ boundary condition was employed to investigate the effect of core density on the

shock response of the curved sandwich panels as well as the damage progression in sandwich panels. The effect of core density on shock response was analyzed under ‘LS’ shock intensity. And, more intense shock, labeled ‘HS’, which had an approximate incident shock peak pressure magnitude of 0.8 MPa, was only used to induce damage in the sandwich panels with high-density core. Compressed nitrogen gas was used in the driver section of the shock tube for the ‘LS’ intensity loading. In contrast, a 70:30 pressure ratio blend of Helium-Nitrogen gas facilitated the ‘HS’ shock loading.

Experimental Methodology

The sandwich composite specimens, with their convex surfaces facing the shock tube muzzle, were secured using fixtures designed to simulate the boundary condition BC1 or BC2. To generate the shock waves of the ‘LS’ intensity, the driver section of the shock tube was pressurized with Nitrogen gas. A Helium and Nitrogen gas mixture was utilized for the ‘HS’ intensity shock.

Stereo Digital Image Correlation (DIC) was employed to quantify the deformations on the back facesheet of the sandwich panels, the side furthest from the loading end. Photron Fastcam Nova S12 cameras equipped with a 60 mm AF micro Nikkor lens (from Nikon, Japan) were used to acquire high-speed images. These cameras captured images at 25,000 frames per second with a pixel resolution of 768×640 . A Photron Fastcam SA1.1 camera featuring a 105 mm AF-DC Nikkor lens (also from Nikon, Japan) was also positioned perpendicular to the shock tube’s axis. Its purpose was to record any deformation and damage within the core. This camera operated at 20,000 frames per second and provided a pixel resolution of 192×832 . The DIC analysis of the panel deformation was performed using a commercial software package: VIC 3D ver.9, developed by Correlated Solutions, located in Columbia, South Carolina.

Dynamic pressure sensors (Models 113B22 & 102B04) from PCB Piezotronics were employed to measure the shock pressure. Pressure data acquisition was recorded using a Tektronix digital oscilloscope (Model: DPO 3034), operating at a 25 MS/s sampling rate. The trigger output from the

oscilloscope was channeled to the cameras, which prompted the commencement of high-speed image recording.

Table 2 provides a comprehensive overview of the experiments presented in this study. The data encompasses both the associated loads and the boundary conditions. Each specimen is designated in the table using the format X-HYYY-ZZ: ‘X’ signifies whether the panel is A, B, or C (as illustrated in Fig. 3); ‘YYY’ represents the nominal core density in kg/m^3 ; and ‘ZZ’ indicates the panel’s serial number. The sandwich panels with low-density core were also subjected to ‘LS’ shock load under boundary condition ‘BC2’. However, the obtained results were similar to the experimental results presented here and, therefore, not included in this manuscript to maintain brevity.

Results and Discussion

The results obtained from these experiments were compared to understand:

1. The interplay between a planar shock front and a curved structure.
2. The influence of curvature on structural response under varied boundary conditions.
3. The impact of core density on the structural response.
4. Damage progression and postmortem observations in sandwich panels.

Interaction of Shock Wave with Curved Geometries

In the shock tube, both the incident and reflected shock pressures acting on the sandwich specimen were measured using the pressure sensor ‘S1’ positioned on the shock tube muzzle [23]. Under normal incidence, the reflected shock pressure, P_0 , is influenced solely by the incident shock strength (represented as $y = P_i/P_{atm}$) and the ratio of the specific heat constants (given as $\mu = C_p/C_v$), as shown in equations (3) and (4).

$$\frac{P_0}{P_i} = \frac{(2\mu + 1)y - \mu}{\mu y + 1} \quad (3)$$

Table 2 List of experiments

Exp. No.	Specimen	Load	BC	Exp. No.	Specimen	Load	BC
1	A-H130-01	LS	BC1	7	A-H045-01	LS	BC1
2	B-H130-01	LS	BC1	8	B-H045-01	LS	BC1
3	C-H130-01	LS	BC1	9	C-H045-01	LS	BC1
4	A-H130-02	LS	BC2	10	A-H130-03	HS	BC1
5	B-H130-02	LS	BC2	11	B-H130-03	HS	BC1
6	C-H130-02	LS	BC2	12	C-H130-03	HS	BC1

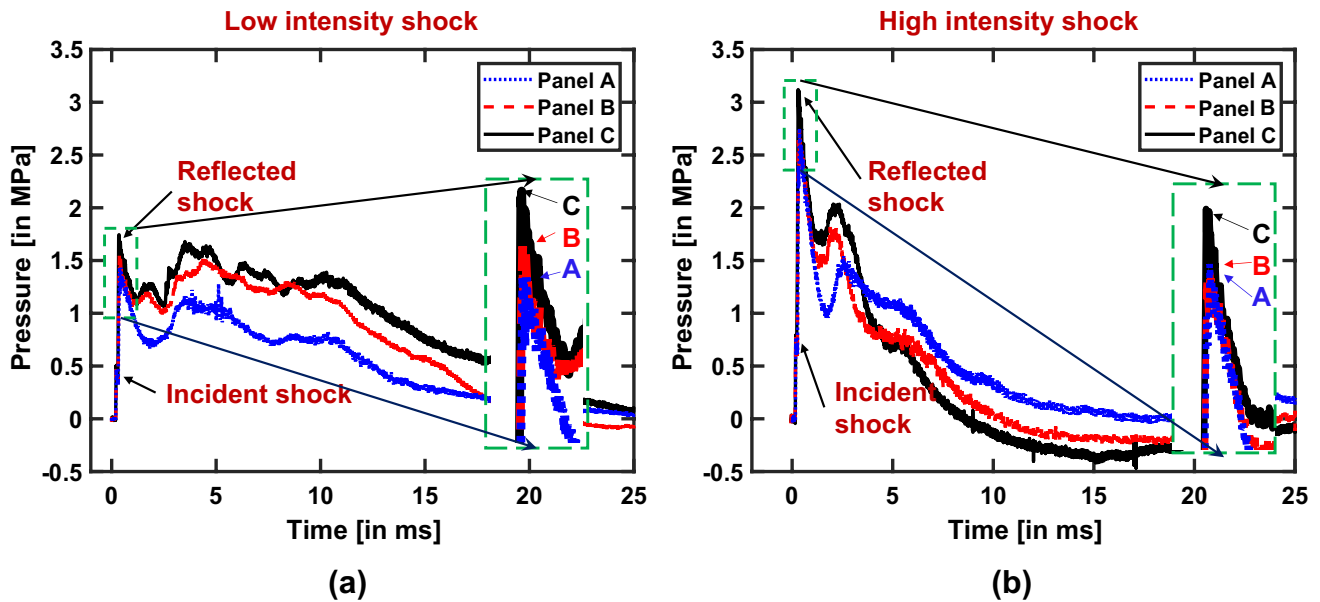


Fig. 5 Typical pressure–time history for shock loading (a) Low intensity (b) High intensity

$$\mu = \frac{\gamma - 1}{\gamma + 1} \quad (4)$$

Uniformity in the shock loading applied to the sandwich panels was validated by assessing the recorded incident shock pressure. Figure 5 delineates typical pressure profiles for Panels A, B, and C when subjected to low (LS) and high-intensity (HS) shock loadings. The incident shock pressures for all panels A, B, and C were found to have the same magnitude for the specified shock load intensities. Nevertheless, the reflected peak pressure, recorded via the muzzle sensor ‘S1’, manifested variations. Panel A exhibited the lowest reflected pressure, while Panel C registered the highest.

The observed differences in the reflected pressure peaks can be attributed to two primary reasons:

1. The reflection of the planar shock front on the curved sandwich panels resulted in a non-uniform reflected pressure distribution due to oblique interactions.
2. There was a release of high-pressure gas through the gap between the muzzle and the curved panels. This release was notably small for Panel C, leading to a minimal decay of the reflected pressure from the panel surface to sensor ‘S1’ [23].

As a result, the reflected pressure recorded by Sensor ‘S1’ at the muzzle end diminished for Panels A and B. Furthermore, the pressure oscillations witnessed during low-intensity shock loading are believed to be a consequence of fluid–structure interaction. Herein, structural oscillations manifest as pressure peaks the pressure sensor

captures [24]. However, these pressure oscillations were absent when the panel incurred damage during loading. This observation is noticeable in the case of high-intensity shock loading, as illustrated in Fig. 5(b). As emphasized earlier, the reflected pressure from a planar shock front interacting with a cylindrical structure varies across the cylindrical surface. The reduction in reflected pressure due to the interaction of a planar shock with a cylindrically curved structure given by Glasstone et al. [25] was digitized and reproduced in Fig. 6(a). This figure depicts the variation in the pressure ratio P_{θ}/P_o , where P_{θ} is the reflected shock pressure along the cylindrically curved surface, and P_o is the reflected shock pressure under normal incidence, with the angle (θ) subtended at the center of curvature, as shown in Fig. 6(b). Interestingly, the pressure variation can be approximated as $P_{\theta}/P_o = \cos(\theta)$ for angles up to 70° , as shown in Fig. 6(a).

Impulse plays a significant role in the dynamic response of structures subjected to explosive or shock loadings. The magnitude of impulse on the curved panels was analytically quantified. The incident and reflected shock pressure were applied on the curved surface exposed to shock loading from the muzzle of the shock tube. However, due to the proximity of the specimen to the muzzle end, the shock diffraction was ignored. The schematic of a curved panel exposed to planar shock through a circular cross-section is shown in Fig. 6(c). The area of the curved panel, S , which is exposed to air shock emanating from the shock tube muzzle, can be estimated using equation (5), where the angle α , r , and R are $\sin^{-1}(r/R)$, muzzle radius, and radius of curvature of the convex cylindrical surface.

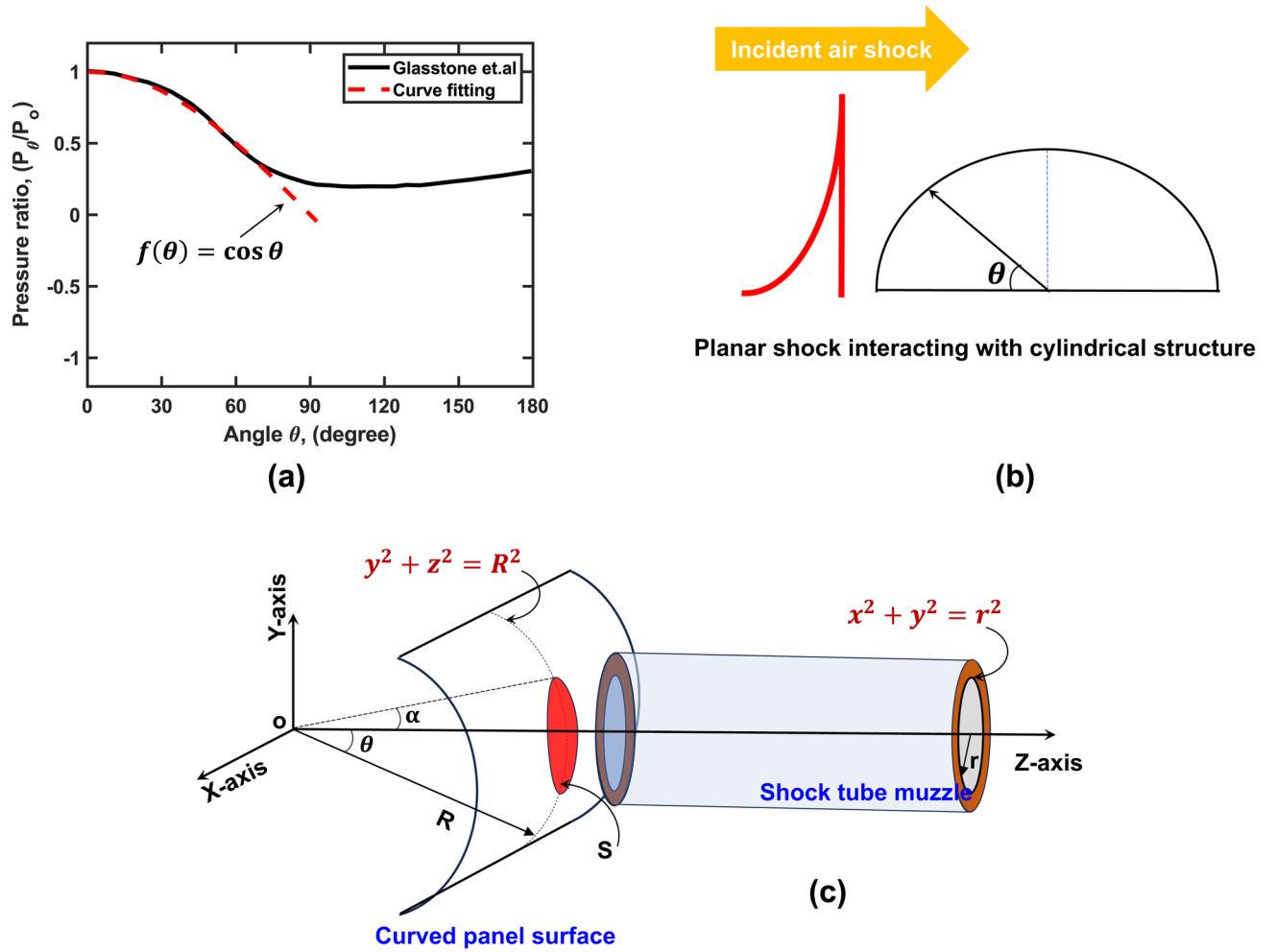


Fig. 6 Reflected shock pressure variation along the cylindrical surface (a) Pressure ratio variation with angle θ (b) Planar shock interaction with cylindrical structure (Schematic) [25] (c) Curved panel exposed to a planar shock through a circular cross-section muzzle (Schematic)

$$A_s = 4R^2 \int_0^\alpha \sqrt{\frac{r^2}{R^2} - \sin^2 \theta} d\theta \quad (5)$$

For curved panels A and B, the panel surface area exposed to shock was calculated by considering ‘ r ’ as 38.1 mm, and ‘ R ’ as 125.5 mm, and 318.5 mm for Panels A and B, respectively. The net pressure distribution at a given instant ‘ t ’ on the cylindrical surface can be mathematically written as $P(t) = P_\theta(t) + P_i(t)$. Due to the symmetry of the curved sandwich panel, the net force acting on the structure is only due to the cosine component of the normal force, i.e., the force component along the direction of the traveling shock, and the net force on a panel at any given instant ‘ t ’ can be mathematically represented by equation (6). Further substituting the results in the expression for instantaneous force, $F(t)$ as shown in equation (7).

$$F(t) = \int_A ((P_o(t)\cos \theta + P_i(t)) \cos \theta) dA \quad (6)$$

$$F(t) = \pi r^2 P_i(t) + 4P_o(t)R^2 \int_0^\alpha \cos^2 \theta \sqrt{\frac{r^2}{R^2} - \sin^2 \theta} d\theta \quad (7)$$

Equation (8) gives the impulse I , transferred to the cylindrical structure during shock loading, which is the time integral of the instantaneous force $F(t)$. The impulse is expressed in terms of the specific impulse (N-s/m²), due to the incident pressure, $I_0^{inc} = \int_0^{T^+} P_i(t) dt$ and reflected pressure, $I_0^{ref} = \int_0^{T^+} P_o(t) dt$ under the normal incidence of shock, for the duration of over-pressure.

$$I = \pi r^2 I_0^{inc} + 4R^2 I_0^{ref} \int_0^\alpha \cos^2 \theta \sqrt{\frac{r^2}{R^2} - \sin^2 \theta} d\theta \quad (8)$$

Table 3 Impulse due to planar shock from the shock tube

Sandwich Panel	Impulse (N-s)	Normalized impulse
Panel A	$4560.4I_0^{inc} + 4507.2I_0^{ref}$	0.993
Panel B	$4560.4I_0^{inc} + 4552.2I_0^{ref}$	0.999
Panel C	$4560.4(I_0^{inc} + I_0^{ref})$	1

The results of the net impulse transferred to the two curved sandwich panels normalized by the impulse transferred to the flat sandwich panel are given in Table 3. The difference in the normalized impulse on the sandwich panels considered in this study is marginal. It suggests that even though the curved panels A and B had a non-uniform pressure distribution due to the oblique reflection of the planar shock wave, the net effect in terms of impulse was not significantly different from that of Panel C, as outlined in Table 3.

Despite the individual pressure variations due to curvature, the net force applied by the shockwave on the panels over the shock duration remained same. Panel C, which had the least curvature and thus experienced more of a head-on

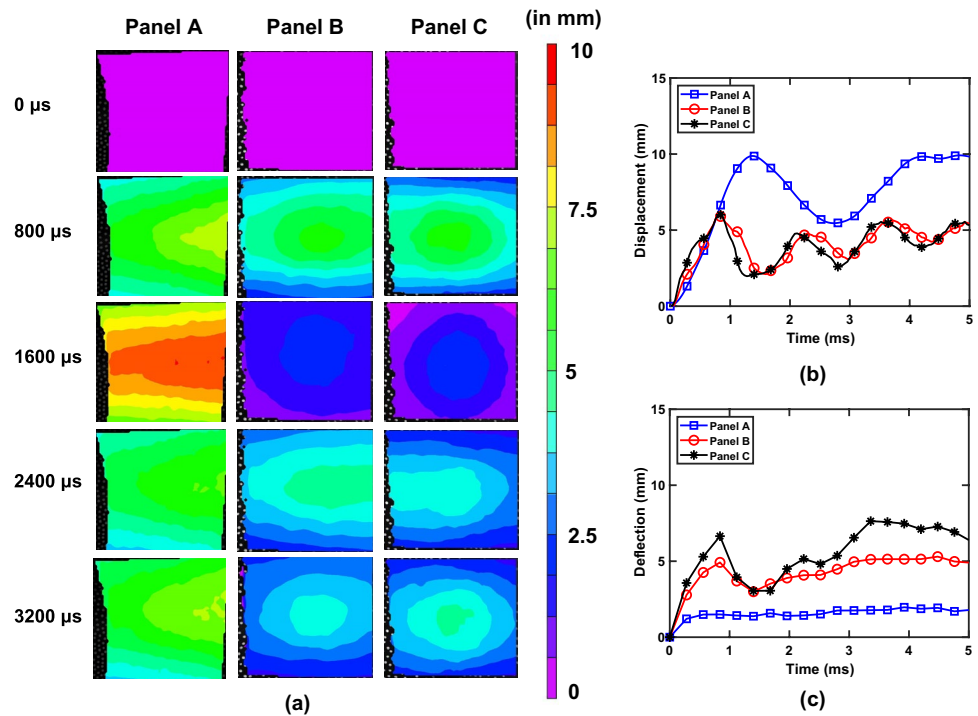
shockwave, had a marginal increase of less than 1% in impulse compared to Panel A.

Effect of Curvature On Structural Response Under Simply Supported and Restricted Boundary Conditions

To comprehend the influence of curvature on the structural behavior of sandwich composites, experiments involving air shock loading were performed on sandwich composite panels (A, B, and C) with a high-density (H130) core and subjected to the ‘BC1’ and ‘BC2’ boundary condition. This study incorporated ‘LS’ intensity load, representing low-intensity shock. The primary objective of the ‘LS’ loading was to capture the blast response of the sandwich panels without causing damage. The incident shock pressure for this experiment series was measured as 0.51 ± 0.03 MPa.

All sandwich panels with boundary conditions ‘BC1’ and ‘BC2’ subjected to the ‘LS’ load displayed oscillatory response following the initial peak displacement, remaining visibly undamaged. Each specimen’s out-of-plane back face deformation (furthest from the shock) was captured using

Fig. 7 DIC results for low-intensity shock loading on curved sandwich panels with high-density PVC closed-cell foam core (a) Out-of-plane displacement contours for low-intensity shock (Typical) (b) Center point out-of-plane displacements for BC1 boundary condition under low-intensity shock loads (c) Center point out-of-plane displacements for BC2 boundary condition under low-intensity shock loads



the stereo DIC camera setup, as detailed in "Experimental Setup" section. Figure 7(a) presents typical deformation profiles of sandwich panels with varying curvatures.

Figure 7(b) shows that for the first 0.5 ms, Panel A displayed the least center point displacement among all the sandwich panels with the 'BC1' boundary condition. The center point displacement was more pronounced for the panel with a larger curvature radius. However, even with the slowest center displacement rate, Panel A displayed the largest initial peak of center point displacement compared to the other panels. Figure 7(c) shows the center point deflection of the sandwich panels following the 'BC2' boundary condition. These sandwich panels registered a deflection magnitude notably lower than the peak deflections observed in panels governed by the 'BC1' boundary.

condition. Also, for the 'BC2' boundary condition, Panel A displayed the least peak deflection compared to the other two panels. This starkly contrasts the behavior noted for 'BC1' boundary conditions, where Panel A demonstrated the maximum peak deflection. Figure 7(c) shows a contrasting pattern in maximum deflection at the center of the specimens with boundary condition 'BC2'. This opposite trend in peak deflections is the influence of the boundary conditions. This change in peak deflection behavior is due to the nonlinear distribution of bending moment along the curved surface, which is more pronounced for the panels with greater angular extent. The angular extent is the angle subtended by the boundary supports at the panel's center of curvature. Xie et al. [26] observed similar behavior in their quasi-static three-point bend tests on curved sandwich beams.

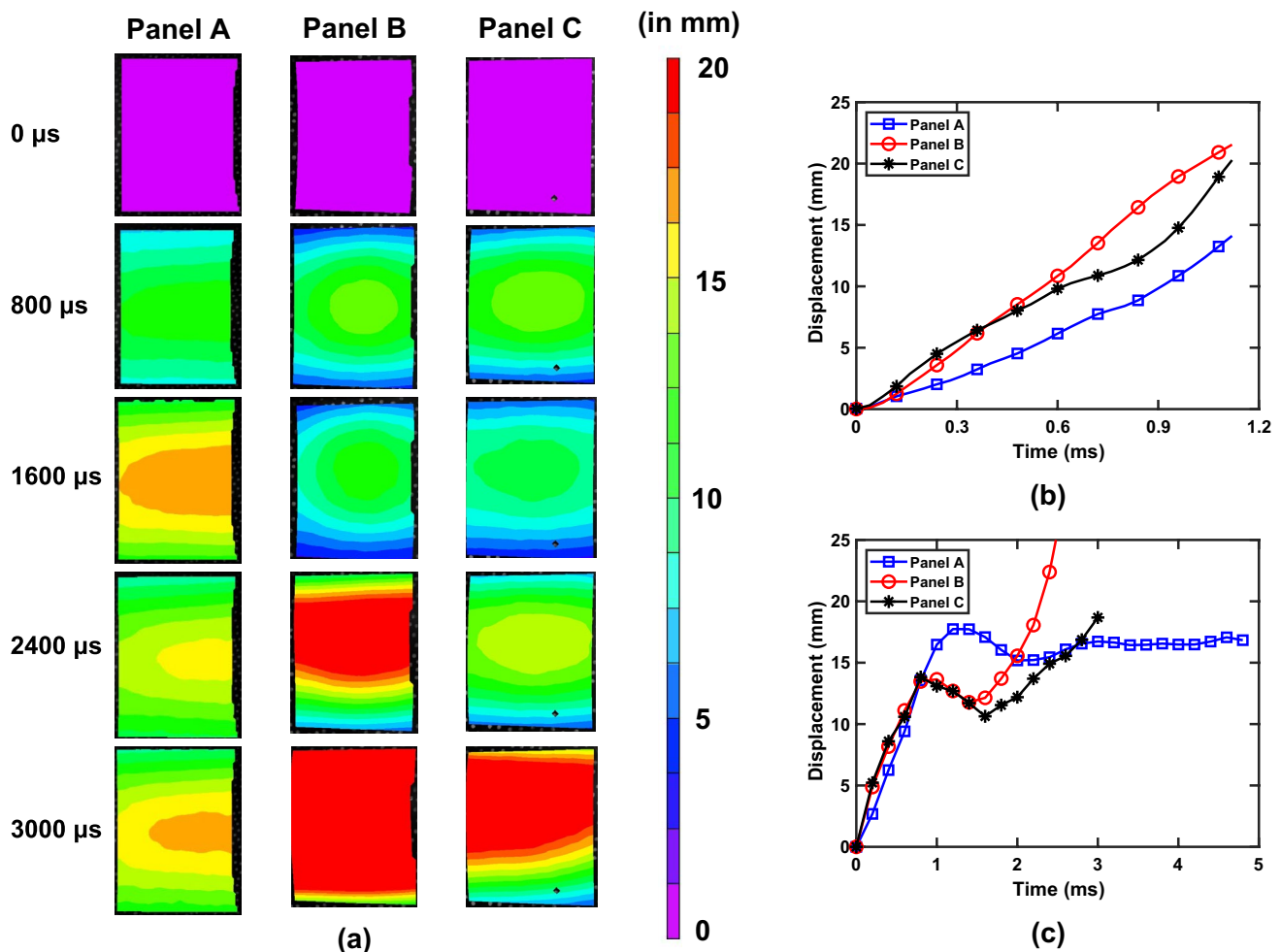


Fig. 8 DIC results for curved sandwich panels with BC1 boundary condition exhibiting damage under shock loading (a) Out-of-plane displacement contours for high-density core sandwich panels (Typical) (b) Center point out-of-plane displacements for low-density (H45) core sandwich panels under low-intensity 'LS' shock loads (c) Center point out-of-plane displacements for high-density (H130) core sandwich panels under high-intensity 'HS' shock loads

Further, the peak displacements with the ‘BC2’ boundary condition, with the diminished deflection of Panel A, are because the net moment at any section under ‘BC2’ is smaller than that under the ‘BC1’ boundary condition. When employing the ‘BC2’ boundary condition, the vertical reaction force counteracts the moment induced by the horizontal reaction force in curved panels. For panels of intermediate curvature, the net bending moment at any given section is also reduced under the ‘BC2’ boundary condition compared to the simple edge support ‘BC1’ boundary condition.

Effect of Core Density On Structural Response

The experiments aimed to discern the influence of core density on the deformation of curved composite sandwich panels. When the panels with a low-density core (H45 PVC closed-cell foam) with ‘BC1’ boundary condition were subjected to ‘LS’ shock loading, they demonstrated a marked reduction in their strength compared to their high-density (H130) counterparts subjected to the same load. The diminished strength of the low-density core panels made them more susceptible to damage even at the given low-intensity ‘LS’ shock load.

The recorded incident shock pressure for these experiments was 0.490 ± 0.024 MPa. All sandwich panels embedded with the H45 core, namely Panels A, B, and C, succumbed to catastrophic failure when subjected to the shock load. This shows the pronounced vulnerability of the panels when the core density is lowered. Further, to estimate the enhanced load capacity of sandwich panels with high-density (H130) core, the specimens Panel A, B, and C with ‘BC1’ boundary conditions were subjected to high-intensity ‘HS’ shock loading. Under the ‘HS’ load condition, Panel A showed no visible damage, while panels B and C showed catastrophic failure.

The deformation patterns exhibited by the low-density core panels resembled those observed in their high-density counterparts. The center point out-of-plane displacement contours for the sandwich panels with the high-density core are shown in Fig. 8(a). The center point displacements extracted from the DIC results for low-density and high-density cores are shown in Fig. 8(b) and (c), respectively. The results shown in Fig. 8(b) and (c) further supported a previously observed trend: Panel A consistently registered the minimum center point displacement rate across all three sandwich panels. The rapid failure of sandwich panels with low-density cores highlights core density's pivotal role in the structural integrity of curved composite sandwich panels under shock loading. Figure 8(c) shows the center point displacements of all three sandwich panels with high-density cores under ‘HS’ intensity shock loading. The deformation trend of Panel A remains consistent, irrespective of core density and shock

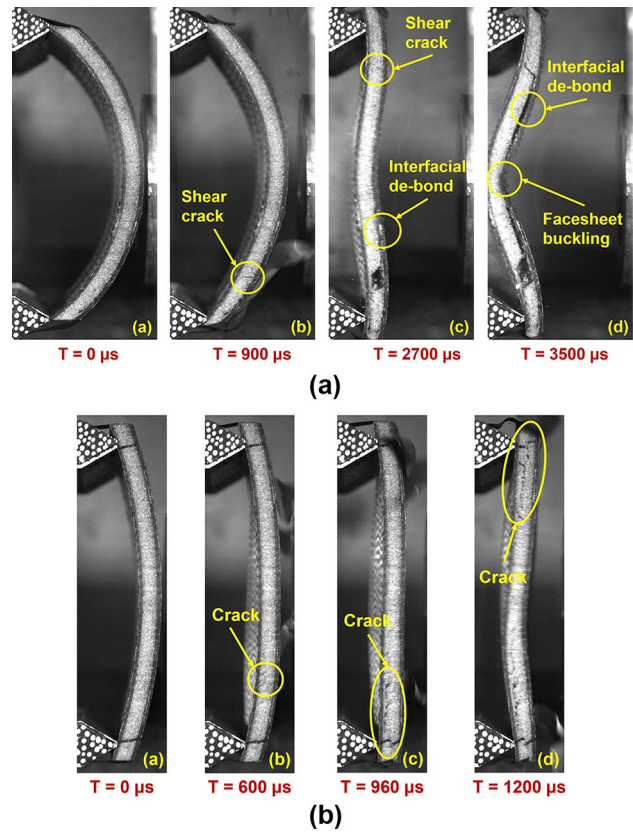


Fig. 9 Damage progression in sandwich panels with low-density closed-cell PVC foam core (a) Panel A (b) Panel B

intensity. The results in Fig. 8 emphasize that while core density is critical in determining the threshold for failure, the intrinsic deformation trend of a panel is influenced by a combination of other factors, including its geometry and boundary conditions.

Hoo Fatt et al. [16] previously illustrated through numerical simulations that for curved sandwich panels with fixed boundary condition, the pressure threshold for failure decreases as the angular extent of the panels increases. Our experimental findings present a different trend from the numerical predictions; the curved panel with a larger angular extent exhibited a higher failure threshold. This deviation may arise from Hoo Fatt et al.’s [16] assumption of a perfectly bonded interface in the numerical simulations.

Damage and Postmortem Observations

The high-speed imaging of the sandwich panels facilitated an understanding of the sequence and mechanisms of failure in these composite materials. The following sub-sections elaborate on the postmortem observations of the sandwich panels with low-density (H45) and high-density (H130) cores.

Sandwich panels with low-density (H45) core

All three sandwich panels, A, B, and C, embedded with low-density core, showed catastrophic failure at ‘LS’ intensity shock loading. Also, panels B and C demonstrated analogous damage progressions with this low-density core. Thus, their response is collectively shown in Fig. 9. Only one of these panels (Panel B) is compared with panel A to highlight the similarities and differences in the failure modes for these curved composite sandwich panels.

Failure in Highest Curvature Sandwich Panel The first visible damage in Panel A was observed as a shear crack within the core at 900 μ s. This crack advanced toward the front and back facesheets and transformed into an interfacial crack upon reaching the facesheet-core interface. As Fig. 9(a) shows, crack propagation eventually led to interfacial de-bonding between the core and facesheet. The separated front facesheet, having lost its stiffness, underwent significant bending, and failed under compressive stress at 3500 μ s.

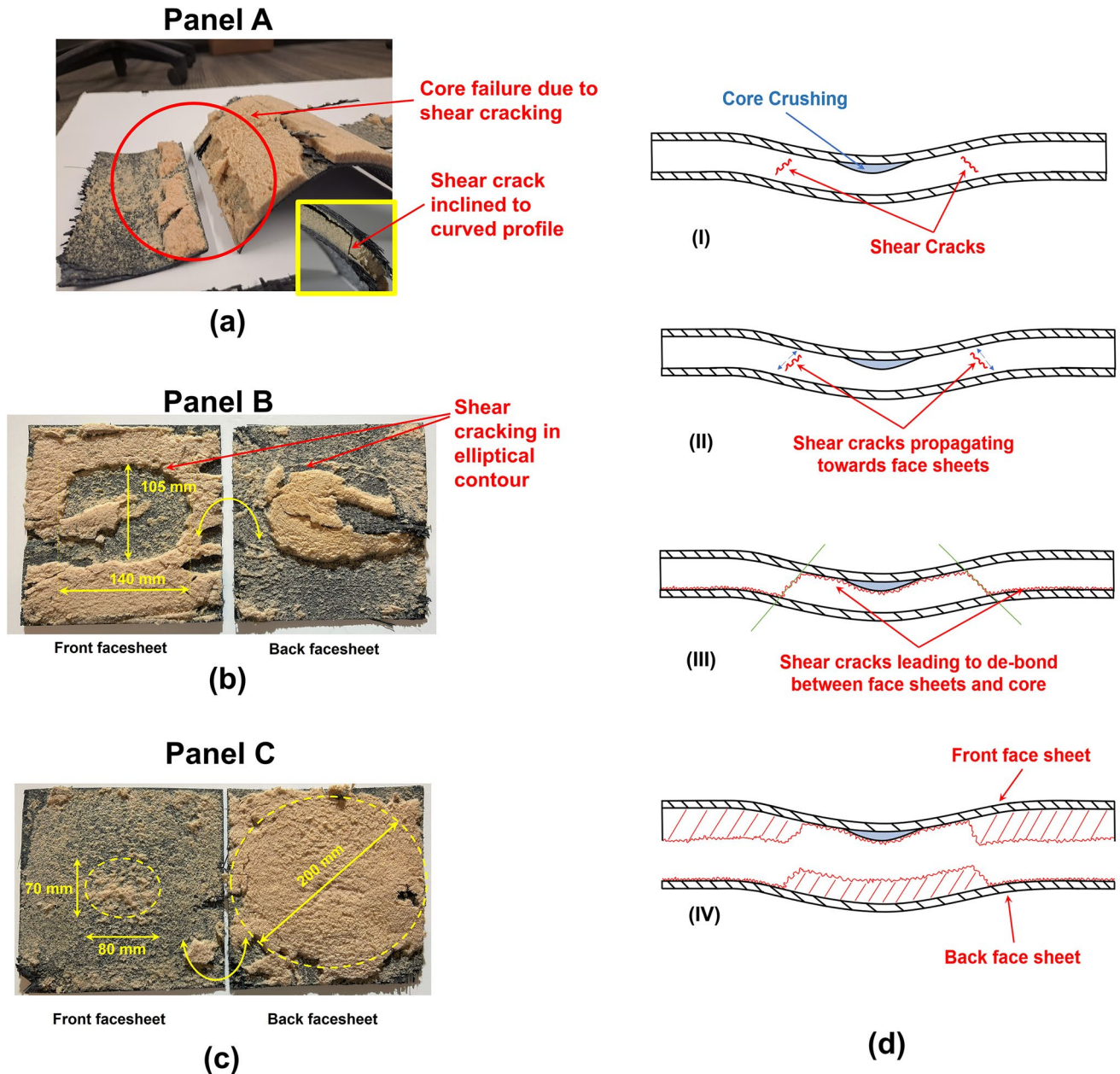


Fig. 10 Postmortem observations on sandwich panels with low-density closed-cell PVC foam core (a) Panel A, (b) Panel B, (c) Panel C (d) Schematic of damage propagation in low-density core sandwich panels

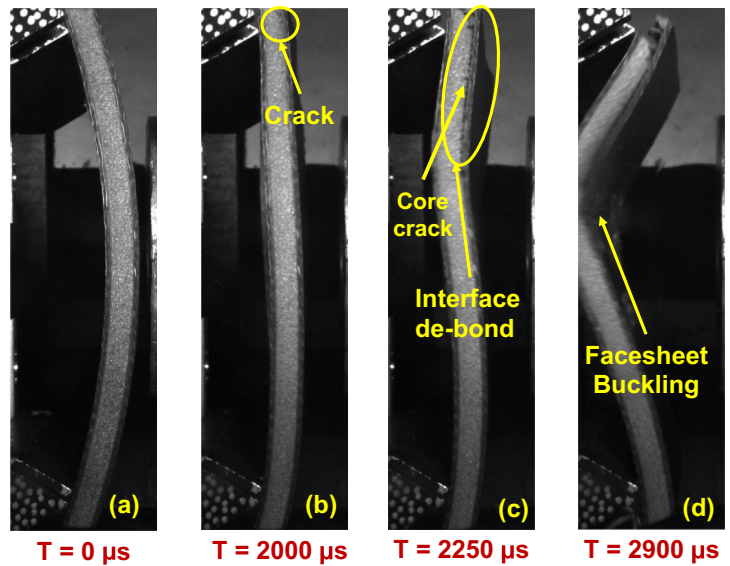
Failure in Intermediate Curvature and Flat Sandwich Panels The onset of damage in Panel B was marked by a crack at 600 μs as seen from the side view camera. This crack was positioned proximate to the back facesheet of the sandwich panel. As it expanded, it vertically split the panel into two sections. A similar pattern of core damage was observed in Panel C. Overall, Panels B and C exhibited damage earlier and more rapidly than Panel A.

Figure 10 presents the images of the damaged sandwich panels comprising a low-density core. A post-examination

of sandwich Panel A highlighted shear cracking along the panel's width. These shear cracks, inclined to the panel's curved profile, were also recorded through high-speed photography, as presented in Fig. 9(a). Panel A did not exhibit core crushing, unlike Panels B and C, which demonstrated evident core crushing during post-test analysis. The core of sandwich Panel B displayed a unique elliptical failure pattern, as depicted in Fig. 10(b). The back facesheet retained an elliptically shaped core segment, creating a matching cavity in the front facesheet exposed to shock loading. A minor foam fragment was also observed at the center of the front

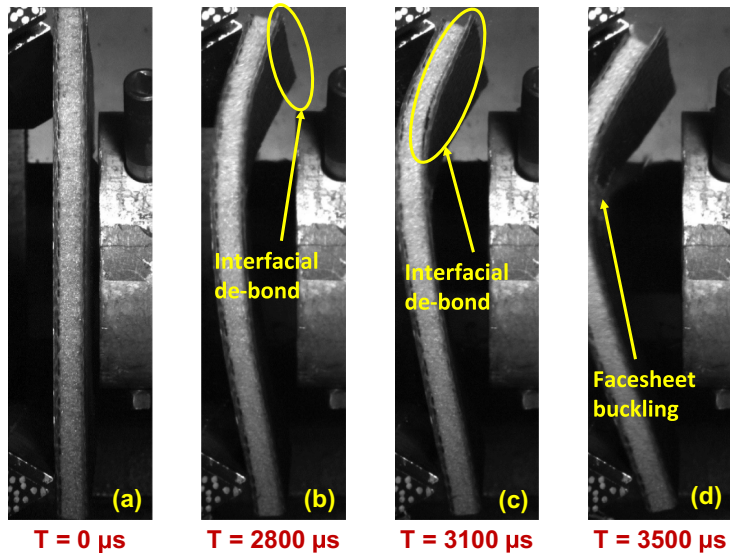
Fig. 11 Damage progression in sandwich composite panels with high-density closed-cell PVC foam core (a) Panel B (b) Panel C

Curved Panel (Panel B)



(a)

Flat Panel (Panel C)



(b)

facesheet. The flat sandwich panel, Panel C, broke into two distinct sections. The core largely remained attached to the back facesheet, leaving traces in the central section and corners of the front facesheet, as illustrated in Fig. 10(c). An elliptical failure contour characterized Panel B's core, while a circular shape was evident in Panel C's core. Figure 10(d) offers a schematic elucidating this elliptical/circular core pattern through a step-by-step damage progression in the sandwich beam, delineating the damage evolution into four distinct phases:

- Stage 1: The shockwave emanating from the shock tube muzzle induces indentation in the low-density core, causing core crushing. Concurrently, specimen deformation occurs, leading to shear cracks within the core.
- Stage 2: These shear cracks extend towards the facesheets, culminating in interfacial cracks.
- Stage 3: These interfacial cracks prompt the interfacial de-bonding between the core and the facesheet over time.

- Stage 4: The aftermath of a failed sandwich beam manifests as a void in the front facesheet, complemented by a corresponding section of the core attached to the back facesheet.

In these experiments, the transverse shock loading on the wide sandwich panels manifests as the failure surface adopting a round geometric shape. The failure contours for Panel B and Panel C shown in Fig. 10(b) and (c) are elliptical and circular geometry. The ellipticity of this contour changes with the curvature-induced stiffness inherent to the sandwich panel.

Furthermore, based on the high-speed imaging and post-mortem observations of sandwich panels (Panel B and Panel C) with a low-density core subjected to 'LS' shock loading under 'BC2' boundary conditions, no discernible effect of boundary conditions was observed on the progression of damage or failure contours.

Besides the direct shock effects, damage to the sandwich panels also stems from the propagation of stress waves through

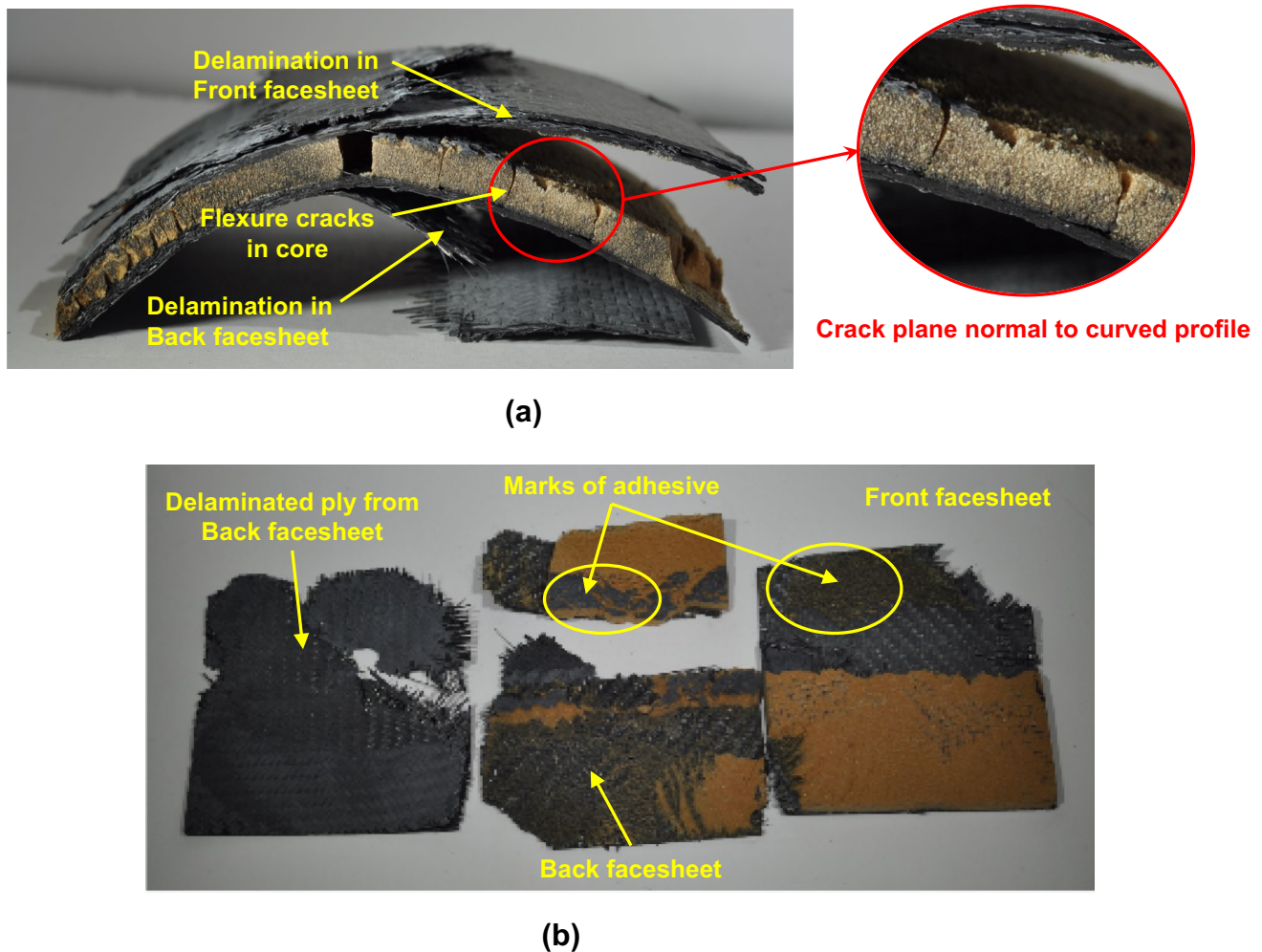


Fig. 12 Postmortem observations on sandwich panels with high-density closed-cell PVC foam core (a) Panel B (b) Panel C

the panel. Damage in the sandwich core was estimated by assuming the linear elastic stress wave propagation through the facesheet and core materials. Analytical results revealed that the stress wave amplitude in the core stands at 90 kPa in compression, a value substantially below the core's crushing strength (600 kPa at a strain rate of $10^3/\text{sec}$, as reported by Wanchoo et al. [27]). Thus, the damage contributed to the core is primarily due to the deformation in sandwich panels.

Sandwich panels with high-density (H130) core

Among the three sandwich panels, the Panel B and C incurred damage and catastrophic failure. However, Panel A didn't exhibit any visible damage. Interestingly, panels B and C both displayed a consistent damage mechanism. Specifically, damage in these panels manifested near the free edge, close to the edge support.

Figure 11(a) shows the damage progression in Panel B. The inception of damage was marked by the first interfacial crack at 2000 μs . This was located at the core-front face sheet interface, near the sandwich panel's free edge. This crack continued to grow along the interface, extending toward the panel's center, leading to an interfacial de-bond between the core and front face sheet. By 2250 μs , cracks within the core, normal to the interface, became noticeable at the core-front face sheet junction. This series of events ultimately resulted in the front face sheet buckling at 2900 μs .

Figure 11(b) depicts the damage evolution in sandwich Panel C. The onset of damage, observed at 2800 μs , similarly began near the free edge and closely aligned with the support location. An interfacial de-bond was observed as this interfacial crack propagated towards the center. This subsequent reduction in stiffness led to the front face sheet of sandwich Panel C buckling by 3500 μs due to the compressive stresses it underwent during bending.

Post-experiment analyses of damaged sandwich Panels B and C, both subjected to the 'HS' shock load, were performed. Figures 12(a) and (b) show the resulting images of these damaged panels. It was noted that no core crushing manifested in Panels B and C, which is characteristic of

high-density cores. The PVC close-cell H130 grade foam (from which the core was made) has a dynamic crushing strength exceeding 3.5 MPa [28]. The peak pressure the 'HS' shock load exerted was approximately 3 MPa, still below this dynamic crushing strength. As a result, the core's deformation remained within the elastic limit. Both sandwich panels predominantly showed de-bonding at the core-face sheet interface as their primary failure mode. Notably, Panel B's core exhibited cracks that opened toward the front face sheet and spread normally to the sandwich panel's curved profile, ultimately extending toward the back face sheet. These cracks, largely attributed to flexural stresses in the core, emerged after the interfacial de-bond at the core-face sheet

interface occurred, a phenomenon captured at 2250 μs , as shown in Fig. 11(a).

Sandwich Panel C, in its post-experiment state shown in Fig. 12(b), exhibited a single flexure crack located centrally. Interfacial de-bond was unmistakably evident, given the adhesive remnants on both the core and the face sheet, further highlighted in Fig. 12(b). Another noteworthy observation was the delamination within the face sheets of both Panels B and C.

Conclusions

This experimental investigation delved into the dynamic behavior of curved composite sandwich panels under shock loading. The study's primary objective was to understand the role of the radius of curvature, core density, and boundary conditions on the dynamic response of a sandwich structure. The out-of-plane displacements on the back face sheet of the sandwich panels were measured using high-speed imaging in tandem with stereo DIC. Concurrently, a high-speed camera on the unsupported side of the sandwich panels captured the damage progression. The research culminated in the following conclusions:

1. The net impulse transferred to the curved sandwich panels was analytically evaluated and the results showed that all the curved sandwich panels (irrespective of the radius of curvature) experienced the same impulse for a given intensity of shock loading.
2. The interplay of panel curvature and boundary conditions strongly influence the sandwich structure's dynamic response. Sandwich panels with simple edge support boundary conditions along the straight edges exhibit an increased deflection for panels with greater angular extent (or lesser radius of curvature). On the other hand, the sandwich panels show a contrasting response when the displacements are arrested at the boundary. The panels with greater angular extent show diminished out-of-plane displacements with arrested displacements at the boundary along straight edges.
3. The sandwich panels with greater angular extent deform at slower rate irrespective of the boundary conditions and the density of core.
4. The core crushing in sandwich composite panels reduces with the increase in the angular extent of the sandwich panel and the core with denser PVC closed-cell foam material.
5. The sandwich panels with higher density cores exhibit enhancement in threshold pressure for interfacial damage and failure for the curved sandwich structures with greater angular extent. In addition, the panel deflections were diminished for higher-density core panels.
6. Damage progression and postmortem observations revealed that the failure mechanism in the sandwich panel changes with the density of PVC closed-cell

foam. However, the boundary conditions do not affect the damage progression and failure surface. The sandwich panels with low-density cores primarily fail from core cracking due to transverse shear stresses. However, this failure mode changes to interfacial de-bond at the core-facesheet interface towards the shock.

Funding The authors gratefully acknowledge the Office of Naval Research (ONR) for the financial support provided under Grant No. N00014-20-1-2877. The authors would also like to acknowledge the DIAB group for providing the PVC foam materials used in the experimental work. The authors are also grateful to their colleagues in the Dynamic Photo-mechanics Laboratory at URI for their support during the experimentation, especially Chris Grivers, Jacob Milman, Jamie Davis, Keevan Winters, and Tyler Chu.

Data Availability The data used in this study will be made available by the corresponding author upon reasonable request.

Declarations

Conflict of Interest The authors certify that they have no affiliations with or involvement in any organization or entity with any financial interest (such as honoraria; educational grants; participation in speakers' bureaus; membership, employment, consultancies, stock ownership, or other equity interest; and expert testimony or patent-licensing arrangements), or non-financial interest (such as personal or professional relationships, affiliations, knowledge or beliefs) in the subject matter or materials discussed in this manuscript.

Open Access This article is licensed under a Creative Commons Attribution 4.0 International License, which permits use, sharing, adaptation, distribution and reproduction in any medium or format, as long as you give appropriate credit to the original author(s) and the source, provide a link to the Creative Commons licence, and indicate if changes were made. The images or other third party material in this article are included in the article's Creative Commons licence, unless indicated otherwise in a credit line to the material. If material is not included in the article's Creative Commons licence and your intended use is not permitted by statutory regulation or exceeds the permitted use, you will need to obtain permission directly from the copyright holder. To view a copy of this licence, visit <http://creativecommons.org/licenses/by/4.0/>.

References

- Mouritz AP, Gellert E, Burchill P, Challis K (2001) Review of advanced composite structures for naval ships and submarines. *Compos Struct* 53:21–42. [https://doi.org/10.1016/S0263-8223\(00\)00175-6](https://doi.org/10.1016/S0263-8223(00)00175-6)
- Wanchoo P, Kishore S, Pandey A, Shukla A (2022) Advances in naval composite and sandwich structures for blast and implosion mitigations. *J Sandwich Struct Mater*. <https://doi.org/10.1177/10996362221139562>
- Birman V, Kardomateas GA (2018) Review of current trends in research and applications of sandwich structures. *Compos B Eng* 142:221–240. <https://doi.org/10.1016/J.COMPOSITESB.2018.01.027>
- Langdon GS, Cantwel WJ, Guan ZW, Nurick GN (2014) The response of polymeric composite structures to air-blast loading: a state-of-the-art. 59:159–77. <https://doi.org/10.1179/1743280413Y.0000000028>
- Wanchoo P, Matos H, Rousseau CE, Shukla A (2021) Investigations on air and underwater blast mitigation in polymeric composite structures – A review. *Compos Struct* 263:113530. <https://doi.org/10.1016/J.COMPSTRUCT.2020.113530>
- Wanchoo P, Pandey A, Leger M, LeBlanc J, Shuka A (2024) Energy quantification framework for underwater explosive loading into PVC foam clad composite plates. *J Mech Phys Solids*. <https://doi.org/10.1016/j.jmps.2024.105646>
- Wang E, Gardner N, Shukla A (2009) The blast resistance of sandwich composites with stepwise graded cores. *Int J Solids Struct* 46:3492–3502. <https://doi.org/10.1016/j.ijsolstr.2009.06.004>
- Wang E, Shukla A (2012) Blast performance of sandwich composites with in-plane compressive loading. *Exp Mech* 52:49–58. <https://doi.org/10.1007/s11340-011-9500-5>
- Gardner N, Wang E, Shukla A (2011) Performance of functionally graded sandwich composite beams under shock wave loading. <https://doi.org/10.1016/j.compstruct.2011.12.006>
- Gardner N, Wang E, Kumar P et al (2012) Blast mitigation in a sandwich composite using graded core and polyurea interlayer. *Exp Mech* 52:119–133. <https://doi.org/10.1007/s11340-011-9517-9>
- Tekalur SA, Bogdanovich AE, Shukla A (2009) Shock loading response of sandwich panels with 3-D woven E-glass composite skins and stitched foam core. *Compos Sci Technol* 69:736–753. <https://doi.org/10.1016/J.COMPSCITECH.2008.03.017>
- Alanbay B, Batra RC (2022) Optimization of blast mitigating sandwich structures with fiber-reinforced face sheets and PVC foam layers as core. *Thin-Walled Struct* 179:109721. <https://doi.org/10.1016/J.TWS.2022.109721>
- Kardomateas GA, Rodcheuy N, Frostig Y (2017) Elasticity solution for curved sandwich beams/panels and comparison with structural theories. *AIAA J* 55:3153–3160. <https://doi.org/10.2514/1.J055760>
- Rodcheuy N, Frostig Y, Kardomateas GA (2017) Extended high-order theory for curved sandwich panels and comparison with elasticity. *J Appl Mech Trans ASME*. <https://doi.org/10.1115/1.4036612/474273>
- Pradyumna S, Nanda N, Bandyopadhyay JN (2010) Geometrically nonlinear transient analysis of functionally graded shell panels using a higher-order finite element formulation. *J Mech Eng Res* 2:39–51
- Fatt MSH, Gao Y, Sirivolu D (2013) Foam-core, curved composite sandwich panels under blast. *J Sandwich Struct Mater* 15:261–291. <https://doi.org/10.1177/1099636213481469>
- Kumar P, Stargel DS, Shukla A (2013) Effect of plate curvature on blast response of carbon composite panels. *Compos Struct* 99:19–30. <https://doi.org/10.1016/J.COMPSTRUCT.2012.11.036>
- Langdon GS, Von Klemperer CJ, Sinclair GM (2016) Blast response of sandwich structures: the influence of curvature. <https://doi.org/10.1016/B978-0-08-100870-6.00013-4>
- Jing L, Wang Z, Shim VPW, Zhao L (2014) An experimental study of the dynamic response of cylindrical sandwich shells with metallic foam cores subjected to blast loading. *Int J Impact Eng* 71:60–72. <https://doi.org/10.1016/J.IJIMPENG.2014.03.009>
- Shen J, Lu G, Wang Z, Zhao L (2010) Experiments on curved sandwich panels under blast loading. *Int J Impact Eng* 37:960–970. <https://doi.org/10.1016/j.ijimpeng.2010.03.002>
- MECHANICAL PROPERTIES DIVINYCELL® H 2023. <https://diab-media.azureedge.net/eyajkrhd/diab-divinycell-h-october-2023-rev23-si.pdf>

22. Full General Datasheet ST 130FR 130 °C TG FIRE RETARDANT LOW SMOKE SPRINT™. <https://www.gurit.com/wp-content/uploads/bsk-pdf-manager/2022/08/ST-130FR.pdf>
23. Wang E, Shukla A (2010) Analytical and experimental evaluation of energies during shock wave loading. *Int J Impact Eng* 37:1188–1196. <https://doi.org/10.1016/J.IJIMPENG.2010.07.003>
24. Wanchoo P, Chaudhary B, Li HWX, Matos H, Shukla A (2023) Blast failure and energy analysis of rubber-modified carbon-fiber vinyl-ester composite laminates. *Mech Mater* 183:104685. <https://doi.org/10.1016/J.MECHMAT.2023.104685>
25. Glasstone S, Dolan PJ (1977) *The effects of nuclear weapons*. Third edition. <https://doi.org/10.2172/6852629>
26. Xie H, Li W, Fang H, Zhang S, Yang Z, Fang Y et al (2024) Flexural behavior evaluation of a foam core curved sandwich beam. *Compos Struct* 328:117729. <https://doi.org/10.1016/J.COMPSTRUCT.2023.117729>
27. Wanchoo P, Pandey A, Shukla A (2023) Stress wave propagation and force transmission in polymeric closed cell foams subjected to air shock loading. *Extreme Mech Lett* 63:102061. <https://doi.org/10.1016/J.EML.2023.102061>
28. Thomas T, Mahfuz H, Carlsson LA, Kanny K, Jeelani S (2002) Dynamic compression of cellular cores: temperature and strain rate effects. *Compos Struct*. [https://doi.org/10.1016/S0263-8223\(02\)00159-9](https://doi.org/10.1016/S0263-8223(02)00159-9)

Publisher's Note Springer Nature remains neutral with regard to jurisdictional claims in published maps and institutional affiliations.